

# 1 Atmospheric Oxidation Mechanism and Kinetics of Indole Initiated 2 by $\cdot\text{OH}$ and $\cdot\text{Cl}$ : A Computational Study

3 Jingwen Xue<sup>1#</sup>, Fangfang Ma<sup>1\*</sup>, Jonas Elm<sup>2</sup>, Jingwen Chen<sup>1</sup>, Hong-Bin Xie<sup>1\*</sup>

4 <sup>1</sup>Key Laboratory of Industrial Ecology and Environmental Engineering (Ministry of Education), School of Environmental  
5 Science and Technology, Dalian University of Technology, Dalian 116024, China

6 <sup>2</sup>Department of Chemistry and iClimate, Aarhus University, Langelandsgade 140, DK-8000 Aarhus C, Denmark

7 *Correspondence to:* Fang-Fang Ma (maff@dlut.edu.cn); Hong-Bin Xie (hbxie@dlut.edu.cn)

8 **Abstract.** The atmospheric chemistry of organic nitrogen compounds (ONCs) is of great importance for understanding the  
9 formation of carcinogenic nitrosamines, and ONC oxidation products might influence atmospheric aerosol particle formation  
10 and growth. Indole is a polyfunctional heterocyclic secondary amine with global emission quantity almost equivalent to that  
11 of trimethylamine, the amine with the highest atmospheric emission. However, the atmospheric chemistry of indole remains  
12 unclear. Herein, the reactions of indole with  $\cdot\text{OH}/\cdot\text{Cl}$ , and subsequent reactions of resulting indole-radicals with  $\text{O}_2$  under 200  
13 ppt NO and 50 ppt  $\text{HO}_2\cdot$  conditions, were investigated by a combination of quantum chemical calculations and kinetics  
14 modeling. The results indicate that  $\cdot\text{OH}$  addition is the dominant pathway for the reaction of  $\cdot\text{OH}$  with indole. However, both  
15  $\cdot\text{Cl}$  addition and H-abstraction are feasible for the corresponding reaction with  $\cdot\text{Cl}$ . All favorably formed indole-radicals further  
16 react with  $\text{O}_2$  to produce peroxy radicals, which mainly react with NO and  $\text{HO}_2\cdot$  to form organonitrates, alkoxy radicals and  
17 hydroperoxide products. Therefore, the oxidation mechanism of indole is distinct from that of previously reported amines,  
18 which primarily form highly oxidized multifunctional compounds, imines or carcinogenic nitrosamines. In addition, the peroxy  
19 radicals from the  $\cdot\text{OH}$  reaction can form N-(2-formylphenyl)formamide ( $\text{C}_8\text{H}_7\text{NO}_2$ ), for the first time providing evidence for  
20 the chemical identity of the  $\text{C}_8\text{H}_7\text{NO}_2$  mass peak observed in the  $\cdot\text{OH}$  + indole experiments. More importantly, this study is  
21 the first to demonstrate that despite forming radicals by abstracting an H-atom at the N-site, carcinogenic nitrosamines were  
22 not produced in the indole oxidation reaction.

## 23 1 Introduction

24 Volatile organic compounds (VOCs) play a central role in air quality and climate change as their transformations are  
25 highly relevant for the formation of secondary organic aerosols (SOA), toxic air pollutants and ozone ( $\text{O}_3$ ) (Ehn et al., 2014;  
26 Karl et al., 2018; Lewis Alastair, 2018; Li et al., 2019; Khare and Gentner, 2018; Ji et al., 2018). Therefore, an accurate  
27 description of the atmospheric transformation mechanism and kinetics of VOCs is essential to fully explore the global impacts  
28 of VOCs. Despite massive effort to understand the atmospheric fate of VOCs, current mechanism-based atmospheric models  
29 often underestimate SOA and  $\text{O}_3$  formation quantity. Therefore, the emission inventories or reaction mechanism employed in

30 the models are either missing some vital primary VOCs or there remain unrevealed reaction mechanism of currently known  
31 VOCs. Hence, it is crucial to identify unaccounted reaction pathways of known VOCs or transformation mechanism of  
32 unconsidered VOCs with high concentrations.

33 Organic nitrogen compounds (ONCs) are a subgroup of VOCs that are widely observed in the atmosphere (Silva et al.,  
34 2008). Until now, about 160 ONCs have been detected in the atmosphere, accounting for 10% of total gas phase nitrogen  
35 (excluding N<sub>2</sub>) (Ge et al., 2011; Silva et al., 2008). Due to the adverse effects of ONCs on air quality (formation of particles  
36 via acid-base reactions or generation of toxic nitrosamines, nitramines, isocyanic acid and low volatile products via gas phase  
37 oxidation), the chemistry of ONCs has gained significant attention in the recent years (Almeida et al., 2013; Chen et al., 2017;  
38 Lin et al., 2019; Nielsen et al., 2012; Zhang et al., 2015; Xie et al., 2014; Xie et al., 2015; Xie et al., 2017; Ma et al., 2018a;  
39 Ma et al., 2021a; Ma et al., 2019; Shen et al., 2019; Shen et al., 2020). Detailed transformation pathways of a series of ONCs  
40 including low-molecular-weight alkyl amines (Nicovich et al., 2015; Xie et al., 2014; Xie et al., 2015; Ma et al., 2021a),  
41 aromatic aniline (Xie et al., 2017; Shiels et al., 2021), heterocyclic amines (Sengupta et al., 2010; Ma et al., 2018a; Borduas et  
42 al., 2016; Ren and Da Silva, 2019) and amides (Xie et al., 2017; Borduas et al., 2016; Borduas et al., 2015; Bunkan et al., 2016;  
43 Bunkan et al., 2015) have been investigated. These studies have shown that the functional groups connected to the NH<sub>x</sub> (x = 0,  
44 1, 2) group highly affect the reactivity of ONCs and eventually lead to their different atmospheric impacts. Therefore, the  
45 comprehensive understanding the reaction mechanism of ONCs with various functional groups linked to the NH<sub>x</sub> group is of  
46 great significance to assess the atmospheric impact of ONCs.

47 Indole is a polyfunctional heterocyclic secondary amine (Laskin et al., 2009). Atmospheric indole has various natural and  
48 anthropogenic sources including vegetation, biomass burning, animal husbandry, coal mining, petroleum processing and  
49 tobacco industry (Ma et al., 2021b; Cardoza et al., 2003; Yuan et al., 2017; Zito et al., 2015). The global emission of indole is  
50 around 0.1 Tg yr<sup>-1</sup> (Misztal et al., 2015), which is almost equivalent to that of trimethylamine (~ 0.17 Tg yr<sup>-1</sup>) (Schade and  
51 Crutzen, 1995; Yu and Luo, 2014) which has the highest emission among the identified atmospheric amines. A field  
52 measurement study found that the concentration of indole can reach 1-3 ppb in ambient air during a springtime flowering event  
53 (Gentner et al., 2014). From a structural point of view, the -NH- group of indole is located at 9-center-10-electron delocalized  
54 π bonds, possibly altering its reactivity compared to that of previously well-studied aliphatic amines and aniline. Therefore,  
55 considering the large atmospheric emission of indole and its unique structure compared to previously studied amines, the  
56 reaction mechanism of indole needs to be further evaluated to assess its atmospheric impacts. Furthermore, elucidating the  
57 reaction mechanism of indole will add to the fundamental understanding of the transformation mechanism of ONCs.

58 Hydroxyl radicals (·OH) are considered to be the most important atmospheric oxidants governing the fate of most organic  
59 compounds (Macleod et al., 2007). Previous experimental studies have investigated the reaction kinetics and identified the  
60 products of the ·OH + indole reaction. Atkinson et al. found that the rate constant (k<sub>OH</sub>-value) of the ·OH + indole reaction is  
61 1.54 × 10<sup>-10</sup> cm<sup>3</sup> molecule<sup>-1</sup> s<sup>-1</sup> at 298 K, translating to a 20 min lifetime of indole (Atkinson et al., 1995). Montoya-Aguilera  
62 et al. found that isatin and isatoic anhydride are the two dominate monomeric products for ·OH initiated reaction of indole.  
63 More importantly, they found that the majority of indole oxidation products can contribute to SOA formation with an effective

64 SOA yield of  $1.3 \pm 0.3$  under the indole concentration (200 ppb) employed in their chamber study (Montoya-Aguilera et al.,  
65 2017). Although the chemical formulas of some of the indole oxidation products have been detected, detailed mechanistic  
66 information such as the products branching ratio of the  $\cdot\text{OH}$  initiated reaction of indole remains unknown. Additionally, the  
67 lack of commercially available standards of some products presents a significant obstacle to identify the exact chemical identity  
68 of the products. Therefore, to fully understand the role of indole in SOA formation, it is essential to investigate the detailed  
69 atmospheric transformation of indole initiated by  $\cdot\text{OH}$ .

70 Besides reactions with  $\cdot\text{OH}$ , reactions with chlorine radicals ( $\cdot\text{Cl}$ ) have been proposed to be an important removal pathway  
71 for ONCs due to the identification of new  $\cdot\text{Cl}$  continental sources and the high reactivity of  $\cdot\text{Cl}$  (Wang et al., 2022; Li et al.,  
72 2021; Jahn et al., 2021; Xia et al., 2020; Young et al., 2014; Faxon and Allen, 2013; Riedel et al., 2012; Atkinson et al., 1989;  
73 Ji et al., 2013; Thornton et al., 2010; Le Breton et al., 2018).  $\cdot\text{Cl}$  initiated atmospheric oxidation of ONCs can lead to the  
74 formation of N-centered radicals, once a strong 2-center-3-electron (2c-3e) bond complex has been formed between  $\cdot\text{Cl}$  and  
75  $\text{NH}_x$  ( $x = 1, 2$ ) (Mckee et al., 1996; Xie et al., 2015; Xie et al., 2017; Ma et al., 2018a). The formed N-centered radicals can  
76 further react with NO to form carcinogenic nitrosamines, increasing the atmospheric impact of ONC emissions (Xie et al.,  
77 2014; Xie et al., 2015; Xie et al., 2017; Ma et al., 2018a; Ma et al., 2021a; Onel et al., 2014a; Onel et al., 2014b; Nielsen et al.,  
78 2012; Da Silva, 2013). As a secondary amine, indole ~~reactions~~reaction with  $\cdot\text{Cl}$  has the possibility of forming N-centered  
79 radicals and subsequently forming nitrosamines via the reaction with NO. Since the -NH- group of indole is embedded in a  
80 unique chemical environment compared to previously well-studied ONCs, the reaction mechanism of  $\cdot\text{Cl}$  with indole remain  
81 elusive. In addition, there are only a few studies concerning the reactions of polyfunctional heterocyclic ONCs with  $\cdot\text{Cl}$ .

82 In this work, we investigated the reaction mechanism and kinetics of indole initiated by  $\cdot\text{OH}$  and  $\cdot\text{Cl}$  by employing a  
83 combination of quantum chemical calculations and kinetic modeling. The initial reactions of  $\cdot\text{OH}/\cdot\text{Cl} + \text{indole}$  and the  
84 subsequent reactions with  $\text{O}_2$  of resulting intermediates were further investigated.

## 85 **2 Computational Details**

### 86 **2.1 Ab Initio Electronic Structure Calculations**

87 All the geometry optimizations and harmonic vibrational frequency calculations were performed at the M06-2X/6-  
88 31+G(d,p) level of theory (Zhao and Truhlar, 2008). Intrinsic reaction coordinate calculations were performed to confirm the  
89 connections of each transition state between the corresponding reactants and products. Single point energy calculations were  
90 performed at the CBS-QB3 method based on the geometries at the M06-2X/6-31+G(d,p) level of theory (Montgomery et al.,  
91 1999). The combination of the M06-2X functional and CBS-QB3 method has successfully been applied to predict radical-  
92 molecule reactions (Guo et al., 2020; Ma et al., 2021b; Wang et al., 2018; Wang and Wang, 2016; Wu et al., 2015; Wang et al.,  
93 2017; Fu et al., 2020).  $T_1$  diagnostic (Table S2) values in the CCSD(T) calculations within the CBS-QB3 scheme for the  
94 intermediates and transition states involved in the key reaction pathways were checked for multireference character. The  $T_1$   
95 diagnostic values for all checked important species in this work are lower than the threshold value of 0.045, indicating the

96 reliability of applied single reference methods (Rienstra-Kiracofe et al., 2000). In addition, similar to our previous studies, a  
97 literature value of 0.8 kcal mol<sup>-1</sup> for the isolated ·Cl was used to account for the effect of spin-orbit coupling in the ·Cl + indole  
98 reaction (Nicovich et al., 2015; Xie et al., 2017; Ma et al., 2018a). Atomic charges of indole and pre-reactive complexes in  
99 the ·Cl + indole reaction are obtained by natural bond orbital (NBO) calculations (Reed et al., 1985). All calculations were  
100 performed within the Gaussian 09 package (Frisch et al., 2009). Throughout the paper, the symbols “R, RC, PC, TS, IM and  
101 P” stand for reactants, pre-reactive complexes, post-reactive complexes, transition states, intermediates and products involved  
102 in the reactions, respectively, and their subscripts denote different species. In addition, “A/B” was used to present the  
103 computational method, where “A” is the theoretical level for single point energy calculations and “B” is that for geometry  
104 optimizations and harmonic frequency calculations.

## 105 2.2 Kinetics Calculations

106 ~~The reaction rate constants for the reactions of ·OH/·Cl + indole and the subsequent reactions of resulting primary~~  
107 ~~intermediates were performed with the MultiWell-2014.1 and MESMER 5.0 programs software were employed to investigate~~  
108 ~~the kinetics for short time and long time reaction, respectively~~ (Barker and Ortiz, 2001; Barker, 2001; Glowacki et al., 2012);  
109 ~~respectively.~~ For the initial reactions with tight transition states of ·OH/·Cl + indole, the reaction kinetics were calculated  
110 within the MultiWell-2014.1 program. For the subsequent reactions of resulting primary intermediates, MESMER 5.0 were  
111 selected for simulating the reaction kinetics, since it has good performance for long time runs, especially for simulating the  
112 variation of the different intermediates over time. Both MultiWell and MESMER codes employs Rice-Ramsperger-Kassel-  
113 Marcus (RRKM) theory ~~within the MultiWell 2014.1 or MESMER 5.0 program was used~~ to calculate the reaction ~~rate~~  
114 ~~constants based on energies and structures at the CBS-QB3//M06-2X/6-31+G(d,p) level of theory~~ kinetics for reactions with  
115 intrinsic energy barriers (Holbrook, 1996; Robinson, 1972). ~~For barrierless entrance pathways (from R to RC), the long~~ Long-  
116 range transition-state theory (LRTST) with a dispersion force potential within the MultiWell-2014.1 program (Barker and  
117 Ortiz, 2001) or Inverse Laplace Transformation (ILT) method within the MESMER 5.0 program was employed to calculate  
118 the reaction rate constants for the barrierless recombination reactions (from R to RC and P to PC) (Rienstra-Kiracofe et al.,  
119 2000). Computational details for performing LRTST and ILT calculation were described in our previous studies (Ma et al.,  
120 2021a; Ma et al., 2021b; Guo et al., 2020; Ding et al., 2020b). The parameters used in the LRTST calculations and Lennard-  
121 Jones parameters of intermediates estimated by the empirical method proposed by Gilbert and Smith (Gilbert, 1990) are listed  
122 in Table S3 and Table S4, respectively. N<sub>2</sub> was selected as the buffer gas, and an average transfer energy of  $\Delta E_d = 200 \text{ cm}^{-1}$   
123 was used to simulate the collision energy transfer between active intermediates and N<sub>2</sub>. In addition,  $\Delta E_d$  between 50 - 250 cm<sup>-1</sup>  
124 were selected to study energy transfer parameters effects. For the reactions involving H-abstraction or H-shift, tunneling  
125 effects were taken into account in all of the reaction rate constants calculations by using a one-dimensional unsymmetrical  
126 Eckart barrier (Eckart, 1930), and were discussed in ~~Supporting Information (the Supporting Information (SI). The kinetic~~  
127 calculations were primarily performed at 298 K and 1 atm, with additional ones at 0.1, 0.4 and 0.7 atm in the troposphere

128 relevant range to explore pressure effects. Variation of the energy transfer parameters and pressure resulted in only minor  
129 changes (< 0.1%) in the calculated rate coefficients and branching ratios of main reaction pathways (see details in the SI).

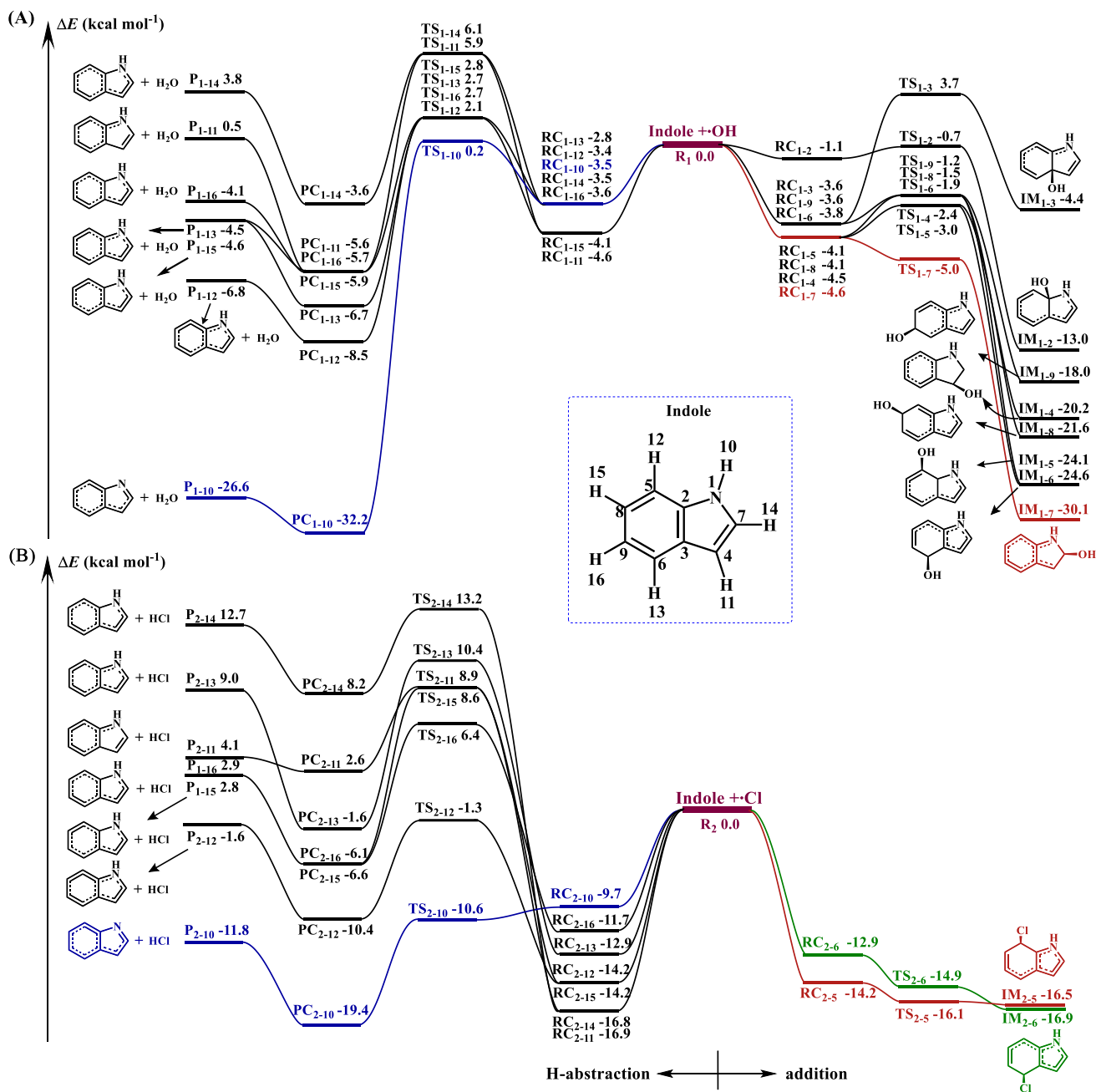
### 130 3 Results and Discussion

#### 131 3.1 Initial Reactions of Indole

132 In principle,  $\cdot\text{OH}$  and  $\cdot\text{Cl}$  could add to the unsaturated C=C bonds and phenyl-groupbenzene ring or directly abstract H-  
133 atoms connected to either to a C-atom or the N-atom of indole. Considering the planar  $C_s$  structure of indole,  $\cdot\text{OH}$  and  $\cdot\text{Cl}$   
134 addition to one side of indole was only considered here. However, although numerous attempts have been made, we failed to  
135 locate the TSs and addition IMs of  $\cdot\text{Cl}$  addition to the C2, C3, C4, C7, C8 and C9 sites of indole-(the numbering of the atoms  
136 is given in Figure 1), suggesting that such additions are in fact unfeasible. Therefore, 7 H-abstraction pathways of  $\cdot\text{OH}$  and  $\cdot\text{Cl}$ ,  
137 respectively, 8  $\cdot\text{OH}$ -addition pathways and 2  $\cdot\text{Cl}$ -addition pathways were considered for the  $\cdot\text{OH}/\cdot\text{Cl}$  + indole reactions. The  
138 schematic zero-point energy (ZPE) corrected potential energy surfaces of  $\cdot\text{OH}/\cdot\text{Cl}$  + indole reactions are presented in Figure  
139 1.

140 As can be seen from Figure 1, each H-abstraction reaction pathway proceeds through a RC and PC, and the addition  
141 pathways through a RC for the  $\cdot\text{OH}/\cdot\text{Cl}$  + indole reactions. For the H-abstraction pathways, the activation energy ( $E_a$ ) for the  
142 -NH- group for both reactions are at least 2.0 kcal mol<sup>-1</sup> lower than the corresponding  $E_a$  values for the -CH- groups. This  
143 indicates that H-abstraction from the -NH- group forming C<sub>8</sub>H<sub>6</sub>N radicals and H<sub>2</sub>O/HCl is the most favorable among all the  
144 H-abstraction pathways. In addition, the activation energy for the H-abstraction from the -NH- group in the  $\cdot\text{Cl}$  + indole  
145 reaction is much lower than the corresponding  $\cdot\text{OH}$  + indole reaction. This is consistent with previously reported reactions of  
146 other amines with  $\cdot\text{OH}$  and  $\cdot\text{Cl}$  (Ma et al., 2018a; Ma et al., 2021a; Xie et al., 2014; Xie et al., 2015; Xie et al., 2017; Tan et  
147 al., 2021; Ren and Da Silva, 2019; Borduas et al., 2015).

148 For the addition reactions, the most favorable reaction site differs for the indole +  $\cdot\text{OH}$  and indole +  $\cdot\text{Cl}$  reactions. Among  
149 all 8  $\cdot\text{OH}$  addition pathways,  $\cdot\text{OH}$  addition to the C7 site of the C=C bond via TS<sub>1-7</sub> forming IM<sub>1-7</sub> is the most favorable  
150 pathway. Different from the reaction with  $\cdot\text{OH}$ , the additions of  $\cdot\text{Cl}$  to the C5 and C6 sites to form IM<sub>2-5</sub> and IM<sub>2-6</sub>, respectively,  
151 are significantly more favorable. By comparing the  $E_a$  values of the addition and H-abstraction pathways for both  $\cdot\text{OH}/\cdot\text{Cl}$  +  
152 indole reactions, it can be concluded that  $\cdot\text{OH}$  addition to the C7 site is the most favorable for the  $\cdot\text{OH}$  + indole reaction. All  
153 the  $\cdot\text{OH}$  + indole hydrogen abstraction reactions have high energy barriers. However, the additions of  $\cdot\text{Cl}$  to the C5 and C6  
154 sites as well as the -NH- H-abstraction are all favorable due to their very lower  $E_a$  values for the  $\cdot\text{Cl}$  + indole reaction.



155

156 **Figure 1: Schematic ZPE-corrected potential energy surface for the reactions of indole + ·OH (A) and indole + ·Cl (B)**  
 157 **at the CBS-QB3//M062X/6-31+g(d,p) level of theory. The total energy of the reactants indole + ·OH/·Cl are set to zero,**  
 158 **respectively (reference state).**

159

160 Interestingly, we found that all the pathways for the indole + ·Cl reaction can proceed via a stable 2c-3e bonded RC,  
 161 which is different from that of the ·OH + indole reaction. Among all 2c-3e bonded RCs, only RC<sub>2-10</sub> from the -NH- abstraction  
 pathway is formed between the N-atom and ·Cl, while the others are formed between the C-atom and ·Cl. Note that RC<sub>2-11</sub>,

162 which forms from C-atom and  $\cdot\text{Cl}$ , is the most stable among all the formed RCs in the  $\cdot\text{Cl}$  + indole reaction. To the best of our  
 163 knowledge, this is the first time that such a stable 2c-3e bonded RC has been identified between the C-atom and  $\cdot\text{Cl}$ . In addition,  
 164 the energy of RC<sub>2-10</sub> is higher than that of the traditional 2c-3e bonded RCs formed from alkylamine and  $\cdot\text{Cl}$ , which would  
 165 result from the delocalization of lone pair electrons of the N-atom. By analyzing the NBO charges of these nine RCs (Table  
 166 S5), we found that significant charge transfer occurs between  $\cdot\text{Cl}$  and indole. The charge at Cl atom for RC<sub>2-5</sub>, RC<sub>2-6</sub>, RC<sub>2-10</sub>,  
 167 RC<sub>2-11</sub>, RC<sub>2-12</sub>, RC<sub>2-13</sub>, RC<sub>2-14</sub>, RC<sub>2-15</sub> and RC<sub>2-16</sub> are  $-0.35 e$ ,  $-0.33 e$ ,  $-0.31 e$ ,  $-0.39 e$ ,  $-0.35 e$ ,  $-0.33 e$ ,  $-0.39 e$ ,  $-0.35 e$  and -  
 168  $0.33e$ , respectively, indicating that all RCs are charge-transfer complexes. Similar charge-transfer complexes were also found  
 169 in our previous study of the  $\cdot\text{Cl}$  + piperazine reaction (Ma et al., 2018a).

170 With the master equation theory, the overall rate constants ( $k_{\text{OH}}$  and  $k_{\text{Cl}}$ ) and branching ratios ( $\Gamma$ ) for all H-abstraction  
 171 and  $\cdot\text{OH}/\cdot\text{Cl}$ -addition pathways involved in the  $\cdot\text{OH}/\cdot\text{Cl}$  + indole reactions were calculated at 298 K and 1 atm. The calculated  
 172  $k_{\text{OH}}$  and  $k_{\text{Cl}}$  values of indole are  $7.9 \times 10^{-11} \text{ cm}^3 \text{ molecule}^{-1} \text{ s}^{-1}$  and  $2.9 \times 10^{-10} \text{ cm}^3 \text{ molecule}^{-1} \text{ s}^{-1}$ , respectively. The calculated  
 173  $k_{\text{OH}}$  value is close to the available experimental value of  $1.5 \times 10^{-10} \text{ cm}^3 \text{ molecule}^{-1} \text{ s}^{-1}$  (Atkinson et al., 1995), supporting the  
 174 reliability of employed computational methods. Over the temperature range 230-330 K (Ma et al., 2018b), the calculated  $k_{\text{OH}}$   
 175 and  $k_{\text{Cl}}$  values have a negative correlation with temperature (Figure S1). Based on the calculated  $\Gamma$  values of the  $\cdot\text{OH}/\cdot\text{Cl}$  +  
 176 indole reactions (Table 1), it can be concluded that IM<sub>1-7</sub> (77%) is the main product for  $\cdot\text{OH}$  + indole reaction, and IM<sub>2-5</sub> (31%),  
 177 IM<sub>2-6</sub> (46%) and P<sub>2-10</sub> (C<sub>8</sub>H<sub>6</sub>N radicals + HCl) (23%) are the main products for  $\cdot\text{Cl}$  + indole reaction. In addition, the calculated  
 178  $\Gamma$  values of IM<sub>1-7</sub>, IM<sub>2-5</sub>, IM<sub>2-6</sub> and P<sub>2-10</sub> (C<sub>8</sub>H<sub>6</sub>N radicals + HCl) change negligibly with the variation of temperature in the  
 179 range of 230-330 K (Figure S2, pressure and energy transfer parameters (SI)). Therefore, we mainly considered the further  
 180 transformation of IM<sub>1-7</sub>, IM<sub>2-5</sub>, IM<sub>2-6</sub> and C<sub>8</sub>H<sub>6</sub>N radicals in the following part.

181 **Table 1. Calculated branching ratios ( $\Gamma$ ) for the indole +  $\cdot\text{OH}/\cdot\text{Cl}$  reactions at 298 K and 1 atm.**

Pathways	Species	$\Gamma$	Species	$\Gamma$	Species	$\Gamma$
$\cdot\text{OH}$ + Indole	IM <sub>1-2</sub>	0	IM <sub>1-3</sub>	0	IM <sub>1-4</sub>	5%
	IM <sub>1-5</sub>	12%	IM <sub>1-6</sub>	3%	IM <sub>1-7</sub>	77%
	IM <sub>1-8</sub>	1%	IM <sub>1-9</sub>	1%	P <sub>1-10</sub>	1%
	P <sub>1-11</sub>	0	P <sub>1-12</sub>	0	P <sub>1-13</sub>	0
	P <sub>1-14</sub>	0	P <sub>1-15</sub>	0	P <sub>1-16</sub>	0
$\cdot\text{Cl}$ + Indole	IM <sub>2-5</sub>	31%	IM <sub>2-6</sub>	46%	P <sub>2-10</sub>	23%
	P <sub>2-11</sub>	0	P <sub>2-12</sub>	0	P <sub>2-13</sub>	0
	P <sub>2-14</sub>	0	P <sub>2-15</sub>	0	P <sub>2-16</sub>	0

### 182 3.2 Subsequent Reactions of Addition Intermediates

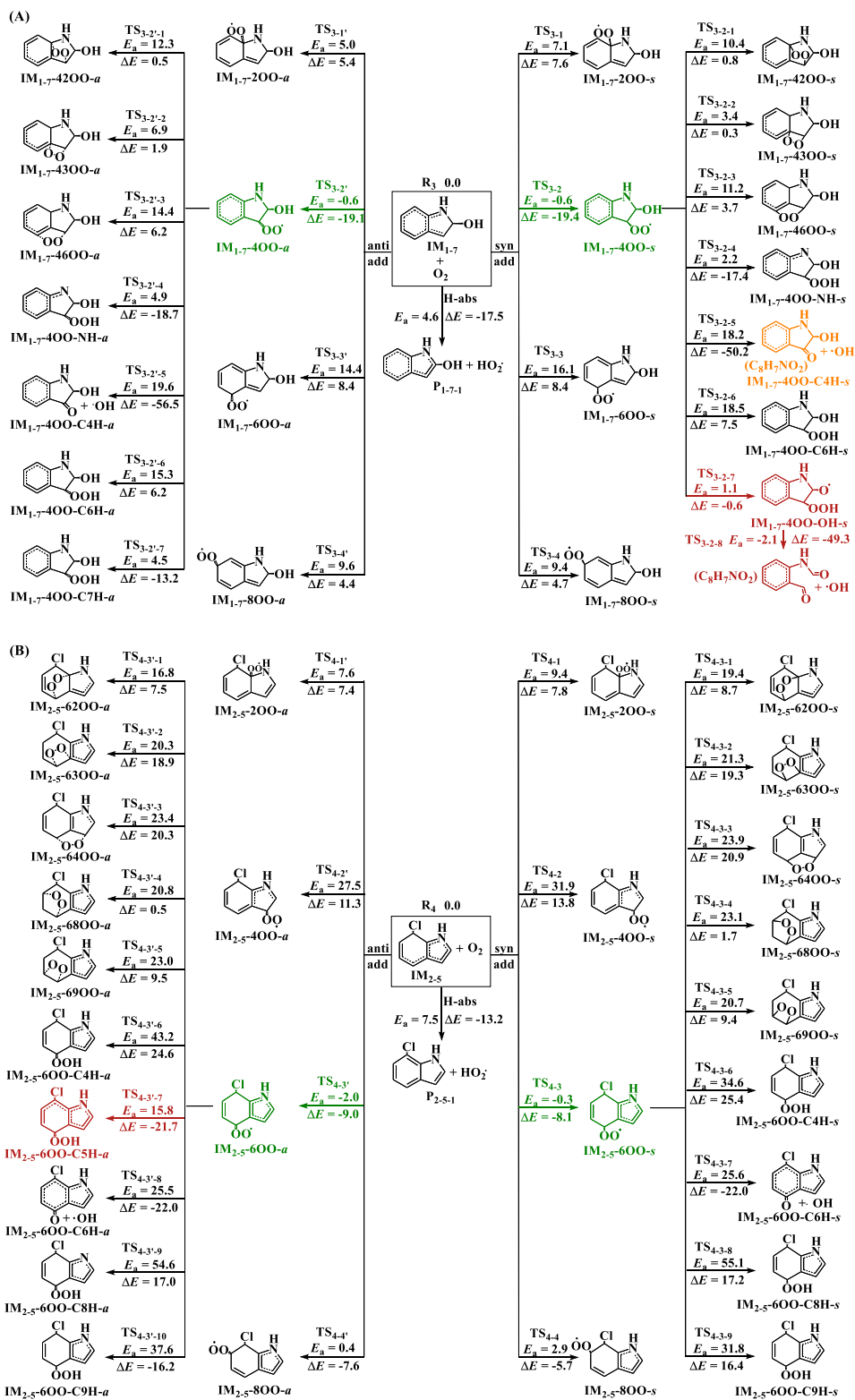
183 Similar to other C-centered radicals (Zhang et al., 2012; Guo et al., 2020; Ma et al., 2021b; Yu et al., 2016; Yu et al., 2017;  
 184 Ji et al., 2017; Ding et al., 2020a), the intermediates IM<sub>1-7</sub>, IM<sub>2-5</sub> and IM<sub>2-6</sub> will subsequently react with O<sub>2</sub>. Two different

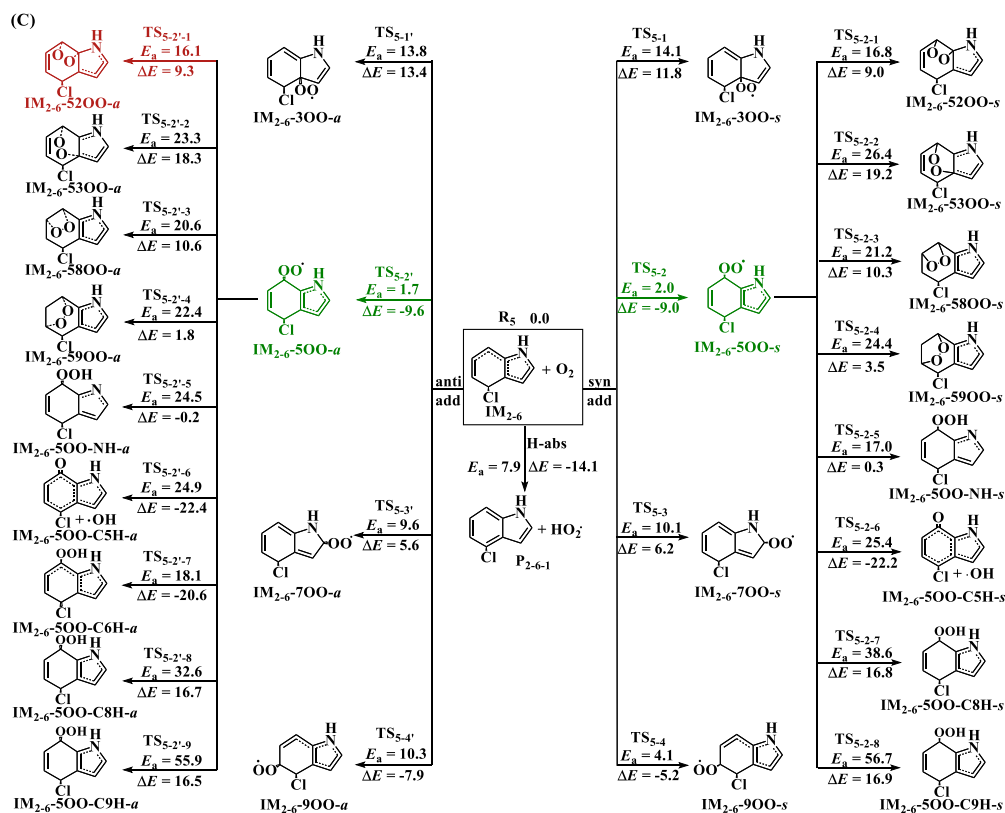
185 pathways (see Figure 2) were considered for the reactions of the intermediates IM<sub>1-7</sub>, IM<sub>2-5</sub> and IM<sub>2-6</sub> with O<sub>2</sub>. One is the direct  
186 hydrogen abstraction by O<sub>2</sub> from the C site connecting to the -OH or -Cl group forming P<sub>1-7-1</sub> (C<sub>8</sub>H<sub>7</sub>NO + HO<sub>2</sub>·), P<sub>2-5-1</sub> (C<sub>8</sub>H<sub>6</sub>NCl  
187 + HO<sub>2</sub>·) and P<sub>2-6-1</sub> (C<sub>8</sub>H<sub>6</sub>NCl + HO<sub>2</sub>·). The other is the O<sub>2</sub> addition to the C sites with high spin density (see spin density  
188 distribution in Table S10) of the intermediates IM<sub>1-7</sub>, IM<sub>2-5</sub> and IM<sub>2-6</sub> to form peroxy radicals *Q-iOO-a/s*, where *Q* stands for  
189 intermediates IM<sub>1-7</sub>, IM<sub>2-5</sub> and IM<sub>2-6</sub>, *i* stands for the numbering of the C-positions where O<sub>2</sub> is added. The O<sub>2</sub> molecule can be  
190 added to the same (-*syn*, abbreviated as -*s*) and opposite (-*anti*, abbreviated as -*a*) sides of the plane relative to -OH or -Cl  
191 group. The C2, C4, C6 and C8 sites of IM<sub>1-7</sub>, C2, C4, C6 and C8 sites of IM<sub>2-5</sub> and C3, C5, C7 and C9 sites of IM<sub>2-6</sub> are high  
192 spin density sites susceptible for O<sub>2</sub> addition.

193 As can be seen from the energetic data shown in Figure 2, O<sub>2</sub> addition to the C4 site of IM<sub>1-7</sub> to form IM<sub>1-7-4OO-a/s</sub> (-  
194 0.6/-0.6 kcal mol<sup>-1</sup>), C6 site of IM<sub>2-5</sub> to form IM<sub>2-5-6OO-a/s</sub> (-0.3/-2.0 kcal mol<sup>-1</sup>) and C5 site of IM<sub>2-6</sub> to form IM<sub>2-6-5OO-a/s</sub>  
195 (2.0/1.7 kcal mol<sup>-1</sup>) are the most favorable among all possible entrance pathways for the respective reactions. It deserves  
196 mentioning that the formation energy ( $\Delta E$ ) of IM<sub>2-5-6OO-a/s</sub> and IM<sub>2-6-5OO-a/s</sub> are only about 9.0 kcal mol<sup>-1</sup>, which could  
197 indicate that they likely re-dissociate back to the reactants IM<sub>2-5</sub>/IM<sub>2-6</sub> and O<sub>2</sub>, if IM<sub>2-5-6OO-a/s</sub> and IM<sub>2-6-5OO-a/s</sub> does not  
198 rapidly transform to other species.

199 For the further transformation of the formed peroxy radicals IM<sub>1-7-4OO(-a/s)</sub>, IM<sub>2-5-6OO(-a/s)</sub> and IM<sub>2-6-5OO(-a/s)</sub>, two  
200 transformation pathways were identified. The first is cyclization reactions where the terminal O-atom of -OO attacks the  
201 different C-positions to form bicycle radicals *Q-ijOO(-a/s)* (*j* stands the number of the C-positions attacked by terminal O-  
202 atom). The second is H-shifts from -OH, -NH- and different -CH- sites to the terminal O-atom to form various hydroperoxide  
203 radicals *Q-iOO-OH(-a/s)*, *Q-iOO-NH(-a/s)* and *Q-iOO-CkH(-a/s)* (*k* stands the number of the C-positions from which H is  
204 shifted), respectively. For IM<sub>1-7-4OO(-a/s)</sub> and IM<sub>2-5-6OO(-a/s)</sub>, forming IM<sub>1-7-4OO-OH-s</sub> and IM<sub>2-5-6OO-C5H-a</sub> via H-shift  
205 reactions are the most favorable, respectively. However, for IM<sub>2-6-5OO(-a/s)</sub>, the cyclization reaction forming IM<sub>2-6-52OO-a</sub>  
206 is the most favorable. It is noted that the formed IM<sub>1-7-4OO-OH-s</sub> from IM<sub>1-7-4OO(-a/s)</sub> can barrierlessly transform to form  
207 C<sub>8</sub>H<sub>7</sub>NO<sub>2</sub> (N-(2-formylphenyl)formamide) and ·OH (collectively denoted P<sub>1-7-4-1</sub>) via concerted C-C and O-O bonds rupture.  
208 The further transformation of the peroxy radicals IM<sub>1-7-4OO(-a/s)</sub>, IM<sub>2-5-6OO(-a/s)</sub> and IM<sub>2-6-5OO(-a/s)</sub> need to overcome  
209 barriers above 20.5 kcal mol<sup>-1</sup> (relative to their respective peroxy radicals), indicating that the further transformation of IM<sub>1-7-</sub>  
210 4OO(-a/s), IM<sub>2-5-6OO(-a/s)</sub> and IM<sub>2-6-5OO(-a/s)</sub> should be very slow.





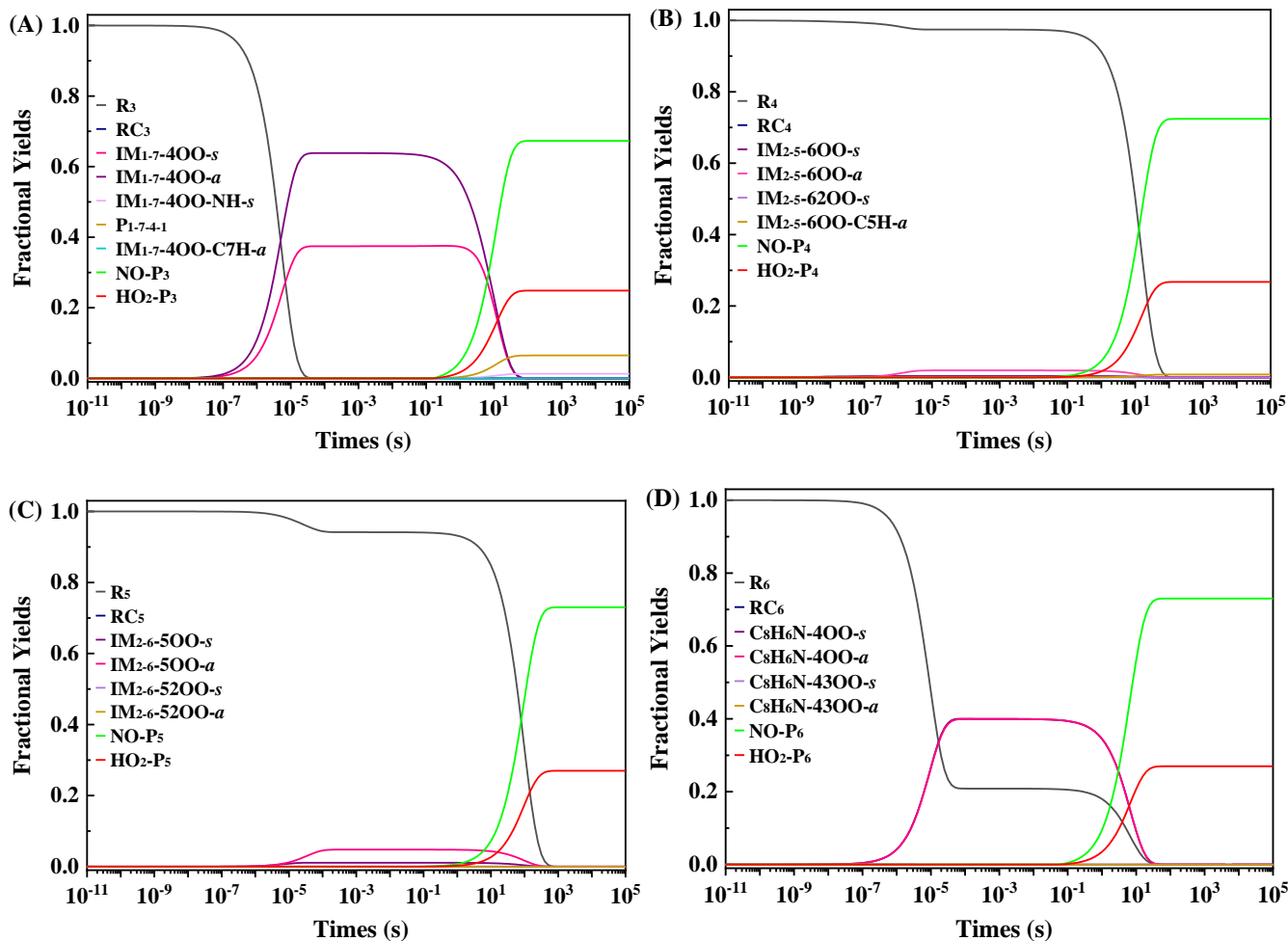


213

214 **Figure 2: Reaction pathways and corresponding energetic data for the reactions of IM<sub>1-7</sub> (A), IM<sub>2-5</sub> (B) and IM<sub>2-6</sub> (C)**  
 215 **with O<sub>2</sub>. Units are in kcal mol<sup>-1</sup>.**

216

217 Based on the energetic data of the favorable reaction pathways, MESMER modeling was employed to investigate the  
 218 reaction rate constants and fractional yields for the reactions of IM<sub>1-7</sub>, IM<sub>2-5</sub>, and IM<sub>2-6</sub> with O<sub>2</sub>. Similar to previous studies  
 219 (Guo et al., 2020; Ma et al., 2021a; Ma et al., 2021b; Zhang et al., 2012; Fu et al., 2020), bimolecular reactions with NO/HO<sub>2</sub>-  
 220 are considered as competitive pathways for the unimolecular reactions of the peroxy radicals IM<sub>1-7</sub>-4OO(-a/s), IM<sub>2-5</sub>-6OO(-  
 221 a/s) and IM<sub>2-6</sub>-5OO(-a/s) by simply adding their pseudo-first-order rate constants into the master equation modeling. Here,  
 222 applied pseudo first order rate constants for peroxy radicals (IM<sub>1-7</sub>-4OO(-a/s), IM<sub>2-5</sub>-6OO(-a/s) and IM<sub>2-6</sub>-5OO(-a/s)) reaction  
 223 with NO and HO<sub>2</sub>· are 0.06 s<sup>-1</sup> and 0.02 s<sup>-1</sup>, respectively, corresponding to reactions occurring at 200 ppt NO and 50 ppt  
 224 HO<sub>2</sub>· conditions (Hofzumahaus et al., 2009; Yu et al., 2020; Praske et al., 2018). The reactions of peroxy radicals with NO and  
 225 HO<sub>2</sub>· should form organonitrate/alkoxy radicals (collectively denoted NO-P<sub>n</sub>, where *n* marks products from the different  
 226 peroxy radical reactions) and hydroperoxide (HO<sub>2</sub>-P<sub>n</sub>), respectively. Pseudo-first-order rate constants of IM<sub>1-7</sub>, IM<sub>2-5</sub>, and IM<sub>2-6</sub>  
 227 with O<sub>2</sub> are calculated to be 3.0 × 10<sup>7</sup> s<sup>-1</sup>, based on the reaction rate constants of IM<sub>1-7</sub>, IM<sub>2-5</sub>, and IM<sub>2-6</sub> with O<sub>2</sub> (6.0 × 10<sup>-12</sup>  
 228 cm<sup>3</sup> molecule<sup>-1</sup> s<sup>-1</sup>) and the concentration of O<sub>2</sub> ([O<sub>2</sub>] = 5.0 × 10<sup>18</sup> molecule cm<sup>-3</sup>). The simulated time-dependent fractional  
 yields are presented in Figure 3.



229

230

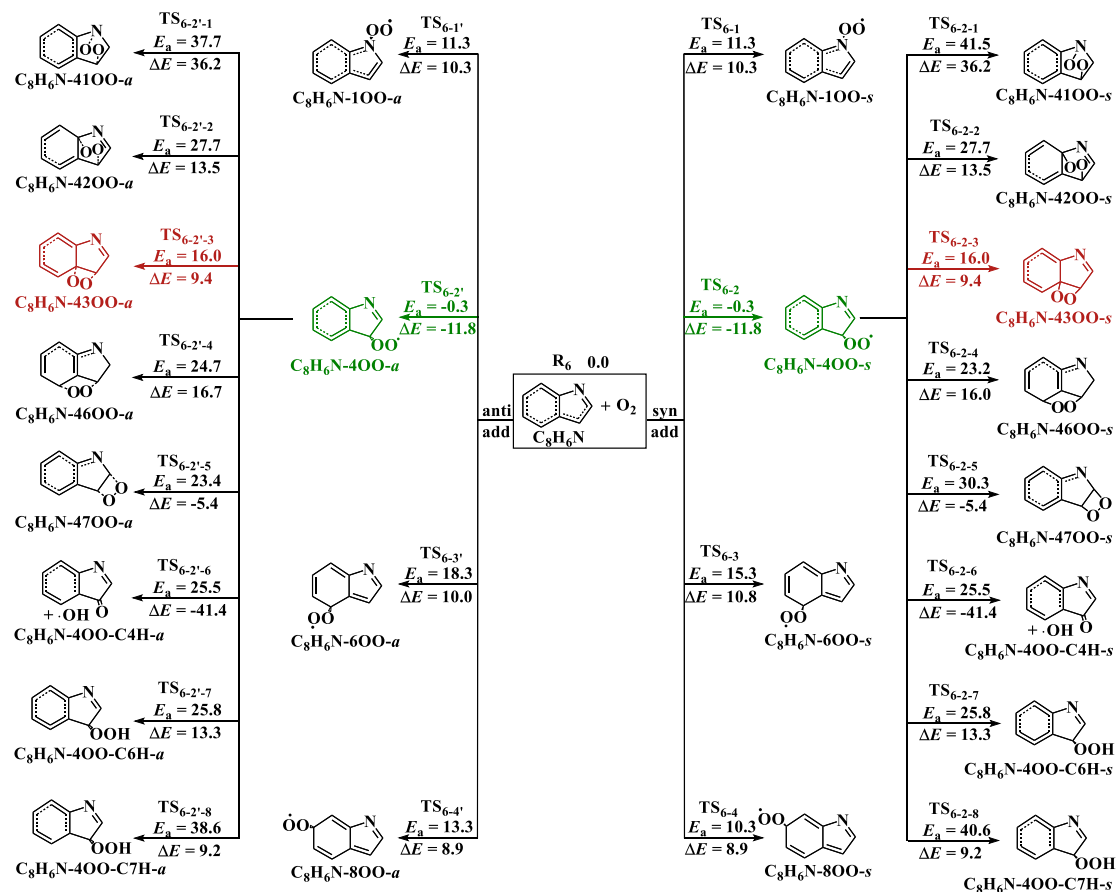
231 **Figure 3: Calculated fractional yields of species (at 200 ppt NO and 50 ppt HO<sub>2</sub>· conditions) as a function of time in the**  
 232 **reactions of IM<sub>1-7</sub> (A), IM<sub>2-5</sub> (B), IM<sub>2-6</sub> (C) and C<sub>8</sub>H<sub>6</sub>N (D) with O<sub>2</sub> at 298 K and 1 atm.**

233 As can be seen in Figure 3, after 100 s, the reactions of IM<sub>1-7</sub>, IM<sub>2-5</sub> and IM<sub>2-6</sub> with O<sub>2</sub> mainly form the organonitrate/alkoxy  
 234 radicals NO-P<sub>3</sub> (C<sub>8</sub>H<sub>8</sub>N<sub>2</sub>O<sub>3</sub>/C<sub>8</sub>H<sub>8</sub>NO<sub>2</sub>·), NO-P<sub>4</sub> (C<sub>8</sub>H<sub>7</sub>N<sub>2</sub>O<sub>3</sub>Cl/C<sub>8</sub>H<sub>7</sub>NCIO·) and NO-P<sub>5</sub> (C<sub>8</sub>H<sub>7</sub>N<sub>2</sub>O<sub>3</sub>Cl/C<sub>8</sub>H<sub>7</sub>NCIO·), followed by  
 235 the formation of hydroperoxide HO<sub>2</sub>-P<sub>3</sub> (C<sub>8</sub>H<sub>9</sub>NO<sub>3</sub>), HO<sub>2</sub>-P<sub>4</sub> (C<sub>8</sub>H<sub>8</sub>NO<sub>2</sub>Cl) and HO<sub>2</sub>-P<sub>5</sub> (C<sub>8</sub>H<sub>8</sub>NO<sub>2</sub>Cl), respectively. For the  
 236 reactions of IM<sub>2-5</sub> and IM<sub>2-6</sub> with O<sub>2</sub>, the main products formed are NO-P<sub>4/5</sub> and HO<sub>2</sub>-P<sub>4/5</sub>. In contrast, the IM<sub>1-7</sub> + O<sub>2</sub> reaction  
 237 also lead to the fragmental products P<sub>1-7-4-1</sub> (C<sub>8</sub>H<sub>7</sub>NO<sub>2</sub> and ·OH) besides the main products NO-P<sub>3</sub> and HO<sub>2</sub>-P<sub>3</sub>. This difference  
 238 in product branching ratios results from the lower unimolecular reaction energy barrier of the peroxy radicals IM<sub>1-7</sub>-400(-a/s)  
 239 from the reaction of IM<sub>1-7</sub> with O<sub>2</sub> than those of IM<sub>2-5</sub>-600(-a/s) and IM<sub>2-6</sub>-500(-a/s) from the reactions of IM<sub>2-5</sub> and IM<sub>2-6</sub>  
 240 with O<sub>2</sub>. It should be noted that the C<sub>8</sub>H<sub>7</sub>NO<sub>2</sub> product has been detected in previous experimental study of the ·OH + indole  
 241 reaction (Montoya-Aguilera et al., 2017), supporting the validity of our computational results.

242 An obvious difference for these three reactions is that the reaction of IM<sub>1-7</sub> with O<sub>2</sub> can form peroxy radicals IM<sub>1-7</sub>-4OO(-  
243 *a/s*) with high yields during the reactions. However, the yields of the corresponding peroxy radicals IM<sub>2-5</sub>-6OO(-*a/s*) and IM<sub>2-6</sub>-  
244 <sub>6</sub>-5OO(-*a/s*) from the reactions of IM<sub>2-5</sub> and IM<sub>2-6</sub> with O<sub>2</sub> are low. The difference mainly originates from the difference in the  
245 formation energy of these three peroxy radicals as shown in Figure 2. The  $\Delta E$  values of IM<sub>1-7</sub>-4OO(-*a/s*)(-19.1/-19.4 kcal mol<sup>-1</sup>)  
246 <sup>1</sup>) are much more lower than those of IM<sub>2-5</sub>-6OO(-*a/s*)(-9.0/-8.1 kcal mol<sup>-1</sup>) and IM<sub>2-6</sub>-5OO(-*a/s*)(-9.6/-9.0 kcal mol<sup>-1</sup>). As  
247 discussed above, the high formation energy of IM<sub>2-5</sub>-6OO(-*a/s*) and IM<sub>2-6</sub>-5OO(-*a/s*) should make IM<sub>2-5</sub>-6OO(-*a/s*) and IM<sub>2-6</sub>-  
248 5OO(-*a/s*) return back to the reactants, explaining the reason for the lower yields of IM<sub>2-5</sub>-6OO(-*a/s*) and IM<sub>2-6</sub>-5OO(-*a/s*).

### 249 3.3 Subsequent Reactions of C<sub>8</sub>H<sub>6</sub>N radicals from the H-abstraction pathway

250 Here, the ~~bi~~molecular**bimolecular** reaction with O<sub>2</sub> was mainly considered for C<sub>8</sub>H<sub>6</sub>N radicals as its sole atmospheric  
251 fate. It was found that the spin density distribution was mainly centered at the C atoms (C4 (0.662), C6 (0.261), C8 (0.178))  
252 and N atom (0.256), indicating that the C<sub>8</sub>H<sub>6</sub>N radical is delocalized. This is in contrast to previously studied N-centered  
253 radicals formed from alkylamines oxidation, which are highly localized (Xie et al., 2015; Xie et al., 2014; Ma et al., 2018a;  
254 Tan et al., 2021; Borduas et al., 2015). Therefore, O<sub>2</sub> addition to the C4, C6, C8 and N1 sites (including attack from both sides)  
255 are considered for the reaction of the C<sub>8</sub>H<sub>6</sub>N radicals with O<sub>2</sub>. As can be seen from Figure 4, O<sub>2</sub> additions to the C4 site of the  
256 C<sub>8</sub>H<sub>6</sub>N radicals forming C<sub>8</sub>H<sub>6</sub>N-4OO-*a/s* with  $E_a$  of -0.3 kcal mol<sup>-1</sup> are the most favorable, translating to pseudo-first-order  
257 reaction rate constants of  $3.0 \times 10^7$  s<sup>-1</sup>. Such rate constants are about 7 orders of magnitude higher than that of typical N-  
258 centered radicals reacting with NO even under very high NO concentration (5 ppb). Therefore, C<sub>8</sub>H<sub>6</sub>N radicals does not react  
259 with NO to form carcinogenic nitrosamines in any appreciable amount, which is different from the previously reported reaction  
260 mechanism of N-centered radicals formed from the reactions of alkylamines with ·Cl (Xie et al., 2015; Xie et al., 2014; Ma et  
261 al., 2018a). To the best of our knowledge, this is the first study to reveal that despite forming radicals by abstracting an H-  
262 atom at the N-site, carcinogenic nitrosamines were not produced in the indole oxidation reaction.



263

264 **Figure 4: Reaction pathways and corresponding energetic data for the reactions of  $C_8H_6N$  radicals with  $O_2$ . Units are**  
 265 **in kcal mol<sup>-1</sup>.**

266 For the transformation of the formed  $C_8H_6N-400-a/s$  radicals, the ring closure reaction to form  $C_8H_6N-4300-a/s$  is the  
 267 most favorable, but still needs to overcome a 27.8 kcal mol<sup>-1</sup> energy barrier, therefore the further transformation of the formed  
 268  $C_8H_6N-400-a/s$  should proceed very slowly. The  $C_8H_6N-400-a/s$  should mainly react with NO and HO<sub>2</sub><sup>·</sup> to form NO-P<sub>6</sub> and  
 269 HO<sub>2</sub>-P<sub>6</sub>. Detailed kinetics calculations (Figure 3D) further confirm that the reaction of  $C_8H_6N$  radicals with  $O_2$  mainly form  
 270 NO-P<sub>6</sub> and HO<sub>2</sub>-P<sub>6</sub> under 200 ppt NO and 50 ppt HO<sub>2</sub><sup>·</sup> conditions.

#### 271 4 Comparison with Available Experimental Results and Atmospheric Implications.

272 This study found that  $\cdot OH/\cdot Cl$  initiated reactions of indole mainly form organonitrates, alkoxy radicals and hydroperoxide  
 273 products with N-(2-formylphenyl)formamide ( $C_8H_7NO_2$ ) as a minor product at 200 ppt NO and 50 ppt HO<sub>2</sub><sup>·</sup> conditions. The  
 274 formed closed-shell products have high oxygen-to-carbon ratios compared to indole and therefore are expected to have lower  
 275 vapor pressures, likely being first generation products that can be further oxidized and contribute to the formation of SOA.

276 With our findings, a comparison was made with the available experimental study on  $\cdot\text{OH}$  initiated reaction of indole. The  
277 calculated  $k_{\text{OH}}$  values ( $7.9 \times 10^{-11} \text{ cm}^3 \text{ molecule}^{-1} \text{ s}^{-1}$ ) of indole is consistent with the experimental value ( $15 \times 10^{-11} \text{ cm}^3$   
278  $\text{molecule}^{-1} \text{ s}^{-1}$ ) (Atkinson et al., 1995), indicating the reliability of applied theoretical methods. A signal with the molecular  
279 formula  $\text{C}_8\text{H}_7\text{NO}_2$  has been observed in the mass spectrum in an experimental study (Montoya-Aguilera et al., 2017),  
280 supporting the formation of the predicted N-(2-formylphenyl)formamide. To the best of our knowledge, this study is the first  
281 to reveal that the chemical identity of the mass spectrum signal as N-(2-formylphenyl)formamide, as opposed to the proposed  
282 3-oxy-2-hydroxy-indole. In addition, monomeric products (isatin and isatoic anhydride) and dimer products has not been  
283 observed in our computational study. We speculate that they may be produced from the subsequent conversion of the formed  
284 alkoxy radicals, multi-generation reactions of organonitrates and hydroperoxide and self/cross reactions of peroxy radicals  
285 ( $\text{RO}_2 + \text{RO}_2$ ). Therefore, further studies are warranted to investigate the subsequent transformation of the formed alkoxy  
286 radicals, organonitrates and hydroperoxide, and the  $\text{RO}_2 + \text{RO}_2$  reactions, to accurately describe the atmospheric impact of  
287 indole.

288 The calculated  $k_{\text{Cl}}$  value of the indole +  $\cdot\text{Cl}$  reaction is a factor of 3.7 higher than that of the indole +  $\cdot\text{OH}$  reaction, and is  
289 close to the  $k_{\text{Cl}}$  values for the reactions of alkylamines, heterocyclic amines and amides with  $\cdot\text{Cl}$  (Xie et al., 2017; Xie et al.,  
290 2015; Ma et al., 2018a; Nicovich et al., 2015). The contribution of  $\cdot\text{Cl}$  to the transformation of indole is calculated to be 3.6-  
291 36% that of  $\cdot\text{OH}$ , assuming  $\cdot\text{Cl}$  concentrations equal to 1-10% of that of  $\cdot\text{OH}$  (Wang and Ruiz, 2017; Nicovich et al., 2015;  
292 Xie et al., 2017; Xie et al., 2015; Ma et al., 2018a). Therefore,  $\cdot\text{Cl}$  plays an important role in the overall transformation of  
293 indole. More importantly,  $\cdot\text{Cl}$  initiated reaction of indole does not lead to the formation of carcinogenic nitrosamines although  
294  $\cdot\text{Cl}$  can favorably abstract the H-atom from N-site to form  $\text{C}_8\text{H}_6\text{N}$  radicals, which is a plausible precursor of carcinogenic  
295 nitrosamines. Hence, to the best of our knowledge, this is the first study to reveal that despite forming radicals by abstracting  
296 an H-atom at the N-site, carcinogenic nitrosamines were not produced in the indole oxidation reaction. This is most likely  
297 caused by the delocalized character of the formed  $\text{C}_8\text{H}_6\text{N}$  radicals due to the existence of the adjacent unsaturated bonds.  
298 Therefore, this study further confirm that the functional groups connected to the  $\text{NH}_x$  ( $x = 1, 2$ ) group highly affect the  
299 atmospheric fate of ONCs. Further studies should be performed to investigate the structure-activity relationship of  $\cdot\text{Cl}$  initiated  
300 reactions of ONCs to comprehensively evaluate their atmospheric impacts.

301

302 *Data availability.* The data in this article are available from the corresponding author upon request (maff@dlut.edu.cn,  
303 hbxie@dlut.edu.cn).

304 *Author contribution.* FFM and HBX designed research; JWX, FFM and HBX performed research; JWX, FFM and HBX  
305 analyzed data; JWX, FFM, JE, HBX and JWC wrote the paper; and FFM, HBX, JE and JWC reviewed and revised the paper.

306 *Competing interests.* The authors declare that they have no conflict of interest.

307 *Acknowledgements.* [We thank Dr. Struan H. Robertson \(Dassault Systèmes\) for the discussion on the MESMER simulations.](#)  
308 The study was supported by the LiaoNing Revitalization Talents Program (XLYC1907194), National Natural Science  
309 Foundation of China (21876024), the Major International (Regional) Joint Research Project (21661142001) and  
310 Supercomputing Center of Dalian University of Technology.

## 311 **References**

- 312 Almeida, J., Schobesberger, S., Kürten, A., Ortega, I. K., Kupiainen-Määttä, O., Praplan, A. P., Adamov, A., Amorim, A.,  
313 Bianchi, F., Breitenlechner, M., David, A., Dommen, J., Donahue, N. M., Downard, A., Dunne, E., Duplissy, J., Ehrhart, S.,  
314 Flagan, R. C., Franchin, A., Guida, R., Hakala, J., Hansel, A., Heinritzi, M., Henschel, H., Jokinen, T., Junninen, H., Kajos,  
315 M., Kangasluoma, J., Keskinen, H., Kupc, A., Kurtén, T., Kvashin, A. N., Laaksonen, A., Lehtipalo, K., Leiminger, M., Leppä,  
316 J., Loukonen, V., Makhmutov, V., Mathot, S., McGrath, M. J., Nieminen, T., Olenius, T., Onnela, A., Petäjä, T., Riccobono,  
317 F., Riipinen, I., Rissanen, M., Rondo, L., Ruuskanen, T., Santos, F. D., Sarnela, N., Schallhart, S., Schnitzhofer, R., Seinfeld,  
318 J. H., Simon, M., Sipilä, M., Stozhkov, Y., Stratmann, F., Tomé, A., Tröstl, J., Tsagkogeorgas, G., Vaattovaara, P., Viisanen,  
319 Y., Virtanen, A., Vrtala, A., Wagner, P. E., Weingartner, E., Wex, H., Williamson, C., Wimmer, D., Ye, P., Yli-Juuti, T.,  
320 Carslaw, K. S., Kulmala, M., Curtius, J., Baltensperger, U., Worsnop, D. R., Vehkamäki, H., and Kirkby, J.: Molecular  
321 understanding of sulphuric acid-amine particle nucleation in the atmosphere, *Nature*, 502, 359-363,  
322 <https://doi.org/10.1038/nature12663>, 2013.
- 323 Atkinson, R., Tuazon, E. C., Arey, J., and Aschmann, S. M.: Atmospheric and indoor chemistry of gas-phase indole, quinoline,  
324 and isoquinoline, *Atmos. Environ.*, 29, 3423-3432, [https://doi.org/10.1016/1352-2310\(95\)00103-6](https://doi.org/10.1016/1352-2310(95)00103-6), 1995.
- 325 Atkinson, R., Baulch, D. L., Cox, R. A., Hampson, R. F., Kerr, J. A., and Troe, J.: Evaluated Kinetic and Photochemical Data  
326 for Atmospheric Chemistry: Supplement III. IUPAC Subcommittee on Gas Kinetic Data Evaluation for Atmospheric  
327 Chemistry, *J. Phys. Chem. Ref. Data*, 18, 881-1097, <https://doi.org/10.1063/1.555832>, 1989.
- 328 Barker, J. R.: Multiple-well, multiple-path unimolecular reaction systems. I. MultiWell computer program suite, *Int. J. Chem.*  
329 *Kinet.*, 33, 232-245, <https://doi.org/10.1002/kin.1017>, 2001.
- 330 Barker, J. R. and Ortiz, N. F.: Multiple-Well, multiple-path unimolecular reaction systems. II. 2-methylhexyl free radicals, *Int.*  
331 *J. Chem. Kinet.*, 33, 246-261, <https://doi.org/10.1002/kin.1018>, 2001.
- 332 Borduas, N., da Silva, G., Murphy, J. G., and Abbatt, J. P. D.: Experimental and Theoretical Understanding of the Gas Phase  
333 Oxidation of Atmospheric Amides with OH Radicals: Kinetics, Products, and Mechanisms, *J. Phys. Chem. A*, 119, 4298-4308,  
334 <https://doi.org/10.1021/jp503759f>, 2015.
- 335 Borduas, N., Abbatt, J. P. D., Murphy, J. G., So, S., and da Silva, G.: Gas-Phase Mechanisms of the Reactions of Reduced  
336 Organic Nitrogen Compounds with OH Radicals, *Environ. Sci. Technol.*, 50, 11723-11734,  
337 <https://doi.org/10.1021/acs.est.6b03797>, 2016.

338 Borduas, N., Murphy, J. G., Wang, C., da Silva, G., and Abbatt, J. P. D.: Gas Phase Oxidation of Nicotine by OH Radicals:  
339 Kinetics, Mechanisms, and Formation of HNCO, *Environ. Sci. Technol. Lett.*, 3, 327-331,  
340 <https://doi.org/10.1021/acs.estlett.6b00231>, 2016.

341 Bunkan, A. J. C., Mikoviny, T., Nielsen, C. J., Wisthaler, A., and Zhu, L.: Experimental and Theoretical Study of the OH-  
342 Initiated Photo-oxidation of Formamide, *J. Phys. Chem. A*, 120, 1222-1230, <https://doi.org/10.1021/acs.jpca.6b00032>, 2016.

343 Bunkan, A. J. C., Hetzler, J., Mikoviny, T., Wisthaler, A., Nielsen, C. J., and Olzmann, M.: The reactions of N-  
344 methylformamide and N,N-dimethylformamide with OH and their photo-oxidation under atmospheric conditions:  
345 experimental and theoretical studies, *Phys. Chem. Chem. Phys.*, 17, 7046-7059, <https://doi.org/10.1039/C4CP05805D>, 2015.

346 Cardoza, Y. J., Lait, C. G., Schmelz, E. A., Huang, J., and Tumlinson, J. H.: Fungus-Induced Biochemical Changes in Peanut  
347 Plants and Their Effect on Development of Beet Armyworm, *Spodoptera Exigua* Hübner (Lepidoptera: Noctuidae) Larvae,  
348 *Environ. Entomol.*, 32, 220-228, <https://doi.org/10.1603/0046-225X-32.1.220>, 2003.

349 Chen, J., Jiang, S., Liu, Y.-R., Huang, T., Wang, C. Y., Miao, S. K., Wang, Z. Q., Zhang, Y., and Huang, W.: Interaction of  
350 oxalic acid with dimethylamine and its atmospheric implications, *RSC Adv.*, 7, 6374-6388,  
351 <https://doi.org/10.1039/C6RA27945G>, 2017.

352 Crounse, J. D., Nielsen, L. B., Jørgensen, S., Kjaergaard, H. G., and Wennberg, P. O.: Autoxidation of Organic Compounds  
353 in the Atmosphere, *J. Phys. Chem. Lett.*, 4, 3513-3520, <https://doi.org/10.1021/jz4019207>, 2013.

354 Ding, Z., Yi, Y., Wang, W., and Zhang, Q.: Atmospheric oxidation of indene initiated by OH radical in the presence of O<sub>2</sub> and  
355 NO: A mechanistic and kinetic study, *Chemosphere*, 259, 127331, <https://doi.org/10.1016/j.chemosphere.2020.127331>, 2020a.

356 Ding, Z., Yi, Y., Wang, W., and Zhang, Q.: Understanding the role of Cl and NO<sub>3</sub> radicals in initiating atmospheric oxidation  
357 of fluorene: A mechanistic and kinetic study, *Sci. Total Environ.*, 716, 136905,  
358 <https://doi.org/10.1016/j.scitotenv.2020.136905>, 2020b.

359 da Silva, G.: Formation of Nitrosamines and Alkyldiazohydroxides in the Gas Phase: The CH<sub>3</sub>NH + NO Reaction Revisited,  
360 *Environ. Sci. Technol.*, 47, 7766-7772, <https://doi.org/10.1021/es401591n>, 2013.

361 Eckart, C.: The penetration of a potential barrier by electrons, *Phys. Rev.*, 35, 1303-1309,  
362 <https://doi.org/10.1103/PhysRev.35.1303>, 1930.

363 Ehn, M., Thornton, J. A., Kleist, E., Sipilä, M., Junninen, H., Pullinen, I., Springer, M., Rubach, F., Tillmann, R., Lee, B.,  
364 Lopez-Hilfiker, F., Andres, S., Acir, I.-H., Rissanen, M., Jokinen, T., Schobesberger, S., Kangasluoma, J., Kontkanen, J.,  
365 Nieminen, T., Kurtén, T., Nielsen, L. B., Jørgensen, S., Kjaergaard, H. G., Canagaratna, M., Maso, M. D., Berndt, T., Petäjä,  
366 T., Wahner, A., Kerminen, V.-M., Kulmala, M., Worsnop, D. R., Wildt, J., and Mentel, T. F.: A large source of low-volatility  
367 secondary organic aerosol, *Nature*, 506, 476-479, <https://doi.org/10.1038/nature13032>, 2014.

368 Faxon, C. B. and Allen, D. T.: Chlorine chemistry in urban atmospheres: a review, *Environ. Chem.*, 10, 221-233,  
369 <https://doi.org/10.1071/en13026>, 2013.



370 Fu, Z., Xie, H. B., Elm, J., Guo, X., Fu, Z., and Chen, J.: Formation of Low-Volatile Products and Unexpected High  
371 Formaldehyde Yield from the Atmospheric Oxidation of Methylsiloxanes, *Environ. Sci. Technol.*, 54, 7136-7145,  
372 <https://doi.org/10.1021/acs.est.0c01090>, 2020.

373 Frisch, M. J., Trucks, G. W., Schlegel, H. B., Scuseria, G. E., Robb, M. A., Cheeseman, J. R., Scalmani, G., Barone, V.,  
374 Mennucci, B., Petersson, G. A., Nakatsuji, H., Caricato, M., Li, X., Hratchian, H. P., Izmaylov, A. F., Bloino, J., Zheng, G.,  
375 Sonnenberg, J. L., Hada, M., Ehara, M., Toyota, K., Fukuda, R., Hasegawa, J., Ishida, M., Nakajima, T., Honda, Y., Kitao, O.,  
376 Nakai, H., Vreven, T., Montgomery, J. A., Jr, Peralta, J. E., Ogliaro, F., Bearpark, M., Heyd, J. J., Brothers, E., Kudin, K. N.,  
377 Staroverov, V. N., Kobayashi, R., Normand, J., Raghavachari, K., Rendell, A., Burant, J. C., Iyengar, S. S., Tomasi, J., Cossi,  
378 M., Rega, N., Millam, J. M., Klene, M., Knox, J. E., Cross, J. B., Bakken, V., Adamo, C., Jaramillo, J., Gomperts, R., Stratmann,  
379 R. E., Yazyev, O., Austin, A. J., Cammi, R., Pomelli, C., Ochterski, J. W., Martin, R. L., Morokuma, K., Zakrzewski, V. G.,  
380 Voth, G. A., Salvador, P., Dannenberg, J. J., Dapprich, S., Daniels, A. D., Farkas, O., Foresman, J. B., Ortiz, J. V., Cioslowski,  
381 J., and Fox, D. J.: *Gaussian 09*, Gaussian Inc., 2009.

382 Ge, X., Wexler, A. S., and Clegg, S. L.: Atmospheric amines – Part I. A review, *Atmos. Environ.*, 45, 524-546,  
383 <https://doi.org/10.1016/j.atmosenv.2010.10.012>, 2011.

384 Gentner, D. R., Ormeño, E., Fares, S., Ford, T. B., Weber, R., Park, J. H., Brioude, J., Angevine, W. M., Karlik, J. F., and  
385 Goldstein, A. H.: Emissions of terpenoids, benzenoids, and other biogenic gas-phase organic compounds from agricultural  
386 crops and their potential implications for air quality, *Atmos. Chem. Phys.*, 14, 5393-5413, [https://doi.org/10.5194/acp-14-](https://doi.org/10.5194/acp-14-5393-2014)  
387 [5393-2014](https://doi.org/10.5194/acp-14-5393-2014), 2014.

388 Glowacki, D. R., Liang, C.-H., Morley, C., Pilling, M. J., and Robertson, S. H.: MESMER: An Open-Source Master Equation  
389 Solver for Multi-Energy Well Reactions, *J. Phys. Chem. A*, 116, 9545-9560, <https://doi.org/10.1021/jp3051033>, 2012.

390 Guo, X., Ma, F., Liu, C., Niu, J., He, N., Chen, J., and Xie, H. B.: Atmospheric oxidation mechanism and kinetics of isoprene  
391 initiated by chlorine radicals: A computational study, *Sci. Total Environ.*, 712, 136330,  
392 <https://doi.org/10.1016/j.scitotenv.2019.136330>, 2020.

393 Holbrook, K. A., Pilling, M. J., Robertson, S. H., and Robinson, P. J.: *Unimolecular Reactions*, 2nd ed, Wiley: New York, 1996.

394 Jahn, L. G., Wang, D. S., Dhulipala, S. V., Ruiz, L. H. et al. Gas-phase chlorine radical oxidation of alkanes: Effects of  
395 structural branching, NO<sub>x</sub>, and relative humidity observed during environmental chamber experiments, *The Journal of Physical*  
396 *Chemistry A*, 125(33): 7303-7317, <https://doi.org/10.1021/acs.jpca.1c03516>, 2021.

397 Ji, Y., Wang, H., Gao, Y., Li, G., and An, T. C.: A theoretical model on the formation mechanism and kinetics of highly toxic  
398 air pollutants from halogenated formaldehydes reacted with halogen atoms, *Atmos. Chem. Phys.*, 13, 11277-11286,  
399 <https://doi.org/10.5194/acp-13-11277-2013>, 2013.

400 Ji, Y., Zheng, J., Qin, D., Li, Y., Gao, Y., Yao, M., Chen, X., Li, G., An, T., and Zhang, R.: OH-Initiated Oxidation of  
401 Acetylacetone: Implications for Ozone and Secondary Organic Aerosol Formation, *Environ. Sci. Technol.*, 52, 11169-11177,  
402 [10.1021/acs.est.8b03972](https://doi.org/10.1021/acs.est.8b03972), 2018.

403 Ji, Y., Zhao, J., Terazono, H., Misawa, K., Levitt, N. P., Li, Y., Lin, Y., Peng, J., Wang, Y., Duan, L., Pan, B., Zhang, F., Feng,  
404 X., An, T., Marrero-Ortiz, W., Secrest, J., Zhang, A. L., Shibuya, K., Molina, M. J., and Zhang, R.: Reassessing the atmospheric  
405 oxidation mechanism of toluene, *Proc. Natl. Acad. Sci. U.S.A.*, 114, 8169, [10.1073/pnas.1705463114](https://doi.org/10.1073/pnas.1705463114), 2017.

406 Karl, T., Striednig, M., Graus, M., Hammerle, A., and Wohlfahrt, G.: Urban flux measurements reveal a large pool of  
407 oxygenated volatile organic compound emissions, *Proc. Natl. Acad. Sci. U.S.A.*, 115, 1186,  
408 <https://doi.org/10.1073/pnas.1714715115>, 2018.

409 Khare, P. and Gentner, D. R.: Considering the future of anthropogenic gas-phase organic compound emissions and the  
410 increasing influence of non-combustion sources on urban air quality, *Atmos. Chem. Phys.*, 18, 5391-5413,  
411 <https://doi.org/10.5194/acp-18-5391-2018>, 2018.

412 Laskin, A., Smith, J. S., and Laskin, J.: Molecular Characterization of Nitrogen-Containing Organic Compounds in Biomass  
413 Burning Aerosols Using High-Resolution Mass Spectrometry, *Environ. Sci. Technol.*, 43, 3764-3771,  
414 <https://doi.org/10.1021/es803456n>, 2009.

415 Le Breton, M., Hallquist, Å. M., Pathak, R. K., Simpson, D., Wang, Y., Johansson, J., Zheng, J., Yang, Y., Shang, D., Wang,  
416 H., Liu, Q., Chan, C., Wang, T., Bannan, T. J., Priestley, M., Percival, C. J., Shallcross, D. E., Lu, K., Guo, S., Hu, M., and  
417 Hallquist, M.: Chlorine oxidation of VOCs at a semi-rural site in Beijing: significant chlorine liberation from ClNO<sub>2</sub> and  
418 subsequent gas- and particle-phase Cl-VOC production, *Atmos. Chem. Phys.*, 18, 13013-13030, [https://doi.org/10.5194/acp-](https://doi.org/10.5194/acp-18-13013-2018)  
419 [18-13013-2018](https://doi.org/10.5194/acp-18-13013-2018), 2018.

420 Hofzumahaus, A., Rohrer, F., Lu, K., Bohn, B., Brauers, T., Chang, C.-C., Fuchs, H., Holland, F., Kita, K., Kondo, Y., Li, X.,  
421 Lou, S., Shao, M., Zeng, L., Wahner, A., and Zhang, Y.: Amplified Trace Gas Removal in the Troposphere, *Science*, 324,  
422 1702-1704, <https://doi.org/10.1126/science.1164566>, 2009.

423 Lewis Alastair, C.: The changing face of urban air pollution, *Science*, 359, 744-745, <https://doi.org/10.1126/science.aar4925>,  
424 2018.

425 Li, J., Zhang, N., Wang, P., Choi, M., Ying, Q., Guo, S., Lu, K., Qiu, X., Wang, S., Hu, M., Zhang, Y., and Hu, J.: Impacts of  
426 chlorine chemistry and anthropogenic emissions on secondary pollutants in the Yangtze river delta region, *Environ. Pollut.*,  
427 287, 117624, <https://doi.org/10.1016/j.envpol.2021.117624>, 2021.

428 Li, K., Li, J., Tong, S., Wang, W., Huang, R. J., and Ge, M.: Characteristics of wintertime VOCs in suburban and urban Beijing:  
429 concentrations, emission ratios, and festival effects, *Atmos. Chem. Phys.*, 19, 8021-8036, [https://doi.org/10.5194/acp-19-8021-](https://doi.org/10.5194/acp-19-8021-2019)  
430 [2019](https://doi.org/10.5194/acp-19-8021-2019), 2019.

431 Lin, Y., Ji, Y., Li, Y., Secrest, J., Xu, W., Xu, F., Wang, Y., An, T., and Zhang, R.: Interaction between succinic acid and  
432 sulfuric acid-base clusters, *Atmos. Chem. Phys.*, 19, 8003-8019, <https://doi.org/10.5194/acp-19-8003-2019>, 2019.

433 Ma, F.F., Xie, H.-B., Li, M., Wang, S., Zhang, R., and Chen, J.: Autoxidation mechanism for atmospheric oxidation of tertiary  
434 amines: Implications for secondary organic aerosol formation, *Chemosphere*, 273, 129207,  
435 <https://doi.org/10.1016/j.chemosphere.2020.129207>, 2021a.

436 Ma, F.F., Xie, H. B., Elm, J., Shen, J., Chen, J., and Vehkamäki, H.: Piperazine Enhancing Sulfuric Acid-Based New Particle  
437 Formation: Implications for the Atmospheric Fate of Piperazine, *Environ. Sci. Technol.*, 53, 8785-8795,  
438 <https://doi.org/10.1021/acs.est.9b02117>, 2019.

439 Ma, F.F., Guo, X. R., Xia, D. M., Xie, H. B., Wang, Y., Elm, J., Chen, J., and Niu, J.: Atmospheric Chemistry of Allylic  
440 Radicals from Isoprene: A Successive Cyclization-Driven Autoxidation Mechanism, *Environ. Sci. Technol.*, 55, 4399-4409,  
441 <https://doi.org/10.1021/acs.est.0c07925>, 2021b.

442 Ma, F.F., Ding, Z. Z., Elm, J., Xie, H. B., Yu, Q., Liu, C., Li, C., Fu, Z., Zhang, L., and Chen, J.: Atmospheric Oxidation of  
443 Piperazine Initiated by  $\cdot\text{Cl}$ : Unexpected High Nitrosamine Yield, *Environ. Sci. Technol.*, 52, 9801-9809,  
444 <https://doi.org/10.1021/acs.est.8b02510>, 2018a.

445 Ma, F.F., Xie, H. B., and Chen, J.: Benchmarking of DFT functionals for the kinetics and mechanisms of atmospheric addition  
446 reactions of OH radicals with phenyl and substituted phenyl-based organic pollutants, *Int. J. Quantum Chem.*, 118, e25533,  
447 <https://doi.org/10.1002/qua.25533>, 2018b.

448 Ma, Q., Meng, N., Li, Y., and Wang, J.: Occurrence, impacts, and microbial transformation of 3-methylindole (skatole): A  
449 critical review, *J. Hazard. Mater.*, 416, 126181, <https://doi.org/10.1016/j.jhazmat.2021.126181>, 2021b.

450 MacLeod, M., Scheringer, M., Podey, H., Jones, K. C., and Hungerbühler, K.: The Origin and Significance of Short-Term  
451 Variability of Semivolatile Contaminants in Air, *Environ. Sci. Technol.*, 41, 3249-3253, <https://doi.org/10.1021/es062135w>,  
452 2007.

453 McKee, M. L., Nicolaides, A., and Radom, L.: A Theoretical Study of Chlorine Atom and Methyl Radical Addition to Nitrogen  
454 Bases: Why Do Cl Atoms Form Two-Center-Three-Electron Bonds Whereas  $\text{CH}_3$  Radicals Form Two-Center-Two-Electron  
455 Bonds, *J. Am. Chem. Soc.*, 118, 10571-10576, <https://doi.org/10.1021/ja9613973>, 1996.

456 Misztal, P. K., Hewitt, C. N., Wildt, J., Blande, J. D., Eller, A. S. D., Fares, S., Gentner, D. R., Gilman, J. B., Graus, M.,  
457 Greenberg, J., Guenther, A. B., Hansel, A., Harley, P., Huang, M., Jardine, K., Karl, T., Kaser, L., Keutsch, F. N., Kiendler-  
458 Scharr, A., Kleist, E., Lerner, B. M., Li, T., Mak, J., Nölscher, A. C., Schnitzhofer, R., Sinha, V., Thornton, B., Warneke, C.,  
459 Wegener, F., Werner, C., Williams, J., Worton, D. R., Yassaa, N., and Goldstein, A. H.: Atmospheric benzenoid emissions  
460 from plants rival those from fossil fuels, *Sci. Rep.*, 5, 12064, <https://doi.org/10.1038/srep12064>, 2015.

461 Montgomery, J. A., Frisch, M. J., Ochterski, J. W., and Petersson, G. A.: A complete basis set model chemistry. VI. Use of  
462 density functional geometries and frequencies, *J. Chem. Phys.*, 110, 2822-2827, <https://doi.org/10.1063/1.477924>, 1999.

463 Montoya-Aguilera, J., Horne, J. R., Hinks, M. L., Fleming, L. T., Perraud, V., Lin, P., Laskin, A., Laskin, J., Dabdub, D., and  
464 Nizkorodov, S. A.: Secondary organic aerosol from atmospheric photooxidation of indole, *Atmos. Chem. Phys.*, 17, 11605-  
465 11621, <https://doi.org/10.5194/acp-17-11605-2017>, 2017.

466 Nicovich, J. M., Mazumder, S., Laine, P. L., Wine, P. H., Tang, Y., Bunkan, A. J. C., and Nielsen, C. J.: An experimental and  
467 theoretical study of the gas phase kinetics of atomic chlorine reactions with  $\text{CH}_3\text{NH}_2$ ,  $(\text{CH}_3)_2\text{NH}$ , and  $(\text{CH}_3)_3\text{N}$ , *Phys. Chem.*  
468 *Chem. Phys.*, 17, 911-917, <https://doi.org/10.1039/C4CP03801K>, 2015.

469 Nielsen, C. J., Herrmann, H., and Weller, C.: Atmospheric chemistry and environmental impact of the use of amines in carbon  
470 capture and storage (CCS), *Chem. Soc. Rev.*, 41, 6684-6704, <https://doi.org/10.1039/C2CS35059A>, 2012.

471 Onel, L., Dryden, M., Blitz, M. A., and Seakins, P. W.: Atmospheric Oxidation of Piperazine by OH has a Low Potential to  
472 Form Carcinogenic Compounds, *Environ. Sci. Technol. Lett.*, 1, 367-371, <https://doi.org/10.1021/ez5002159>, 2014a.

473 Onel, L., Blitz, M., Dryden, M., Thonger, L., and Seakins, P.: Branching Ratios in Reactions of OH Radicals with Methylamine,  
474 Dimethylamine, and Ethylamine, *Environ. Sci. Technol.*, 48, 9935-9942, <https://doi.org/10.1021/es502398r>, 2014b.

475 Praske, E., Otkjær, R. V., Crounse, J. D., Hethcox, J. C., Stoltz, B. M., Kjaergaard, H. G., and Wennberg, P. O.: Atmospheric  
476 autoxidation is increasingly important in urban and suburban North America, *Proc. Natl. Acad. Sci. U.S.A.*, 115, 64,  
477 <https://doi.org/110.1073/pnas.1715540115>, 2018.

478 Reed, A. E., Weinstock, R. B., and Weinhold, F.: Natural population analysis, *J. Chem. Phys.*, 83, 735-746,  
479 <https://doi.org/10.1063/1.449486>, 1985.

480 Ren, Z. and da Silva, G.: Atmospheric Oxidation of Piperazine Initiated by OH: A Theoretical Kinetics Investigation, *ACS*  
481 *Earth Space Chem.*, 3, 2510-2516, <https://doi.org/10.1021/acsearthspacechem.9b00227>, 2019.

482 Riedel, T. P., Bertram, T. H., Crisp, T. A., Williams, E. J., Lerner, B. M., Vlasenko, A., Li, S.-M., Gilman, J., de Gouw, J.,  
483 Bon, D. M., Wagner, N. L., Brown, S. S., and Thornton, J. A.: Nitryl Chloride and Molecular Chlorine in the Coastal Marine  
484 Boundary Layer, *Environ. Sci. Technol.*, 46, 10463-10470, <https://doi.org/10.1021/es204632r>, 2012.

485 Rienstra-Kiracofe, J. C., Allen, W. D., and Schaefer, H. F.: The  $C_2H_5 + O_2$  Reaction Mechanism: High-Level ab Initio  
486 Characterizations, *J. Phys. Chem. A*, 104, 9823-9840, <https://doi.org/10.1021/jp001041k>, 2000.

487 Robinson, P. J., and Holbrook, K. A.: *Unimolecular Reactions*, John Wiley & Sons: New York, 1972.

488 SenGupta, S., Indulkar, Y., Kumar, A., Dhanya, S., Naik, P. D., and Bajaj, P. N.: Kinetics of Gas-Phase Reaction of OH with  
489 Morpholine: An Experimental and Theoretical Study, *J. Phys. Chem. A*, 114, 7709-7715, <https://doi.org/10.1021/jp101464x>,  
490 2010.

491 Schade, G. W. and Crutzen, P. J.: Emission of aliphatic amines from animal husbandry and their reactions: Potential source of  
492  $N_2O$  and HCN, *J. Atmos. Chem.*, 22, 319-346, <https://doi.org/10.1007/BF00696641>, 1995.

493 Shiels, O. J., Kelly, P. D., Bright, C. C., Poad, B. L. J., Blanksby, S. J., da Silva, G., and Trevitt, A. J.: Reactivity Trends in the  
494 Gas-Phase Addition of Acetylene to the N-Protonated Aryl Radical Cations of Pyridine, Aniline, and Benzonitrile, *J. Am. Soc.*  
495 *Mass. Spectrom.*, 32, 537-547, <https://doi.org/10.1021/jasms.0c00386>, 2021.

496 Shen, J., Elm, J., Xie, H.-B., Chen, J., Niu, J., and Vehkamäki, H.: Structural Effects of Amines in Enhancing Methanesulfonic  
497 Acid-Driven New Particle Formation, *Environ. Sci. Technol.*, 54, 13498-13508, <https://doi.org/10.1021/acs.est.0c05358>, 2020.

498 Shen, J., Xie, H.-B., Elm, J., Ma, F., Chen, J., and Vehkamäki, H.: Methanesulfonic Acid-driven New Particle Formation  
499 Enhanced by Monoethanolamine: A Computational Study, *Environ. Sci. Technol.*, 53, 14387-14397,  
500 <https://doi.org/10.1021/acs.est.9b05306>, 2019.

501 Silva, P. J., Erupe, M. E., Price, D., Elias, J., G. J. Malloy, Q., Li, Q., Warren, B., and Cocker, D. R.: Trimethylamine as  
502 Precursor to Secondary Organic Aerosol Formation via Nitrate Radical Reaction in the Atmosphere, *Environ. Sci. Technol.*,  
503 42, 4689-4696, <https://doi.org/10.1021/es703016v>, 2008.

504 Tan, W., Zhu, L., Mikoviny, T., Nielsen, C. J., Wisthaler, A., D'Anna, B., Antonsen, S., Stenstrøm, Y., Farren, N. J., Hamilton,  
505 J. F., Boustead, G. A., Brennan, A. D., Ingham, T., and Heard, D. E.: Experimental and Theoretical Study of the OH-Initiated  
506 Degradation of Piperazine under Simulated Atmospheric Conditions, *J. Phys. Chem. A*, 125, 411-422,  
507 <https://doi.org/10.1021/acs.jpca.0c10223>, 2021.

508 Thornton, J. A., Kercher, J. P., Riedel, T. P., Wagner, N. L., Cozic, J., Holloway, J. S., Dubé, W. P., Wolfe, G. M., Quinn, P.  
509 K., Middlebrook, A. M., Alexander, B., and Brown, S. S.: A large atomic chlorine source inferred from mid-continental  
510 reactive nitrogen chemistry, *Nature*, 464, 271-274, <https://doi.org/10.1038/nature08905>, 2010.

511 Veres, P. R., Neuman, J. A., Bertram, T. H., Assaf, E., Wolfe, G. M., Williamson, C. J., Weinzierl, B., Tilmes, S., Thompson,  
512 C. R., Thames, A. B., Schroder, J. C., Saiz-Lopez, A., Rollins, A. W., Roberts, J. M., Price, D., Peischl, J., Nault, B. A., Møller,  
513 K. H., Miller, D. O., Meinardi, S., Li, Q., Lamarque, J.-F., Kupc, A., Kjaergaard, H. G., Kinnison, D., Jimenez, J. L., Jernigan,  
514 C. M., Hornbrook, R. S., Hills, A., Dollner, M., Day, D. A., Cuevas, C. A., Campuzano-Jost, P., Burkholder, J., Bui, T. P.,  
515 Brune, W. H., Brown, S. S., Brock, C. A., Bourgeois, I., Blake, D. R., Apel, E. C., and Ryerson, T. B.: Global airborne sampling  
516 reveals a previously unobserved dimethyl sulfide oxidation mechanism in the marine atmosphere, *Proc. Natl. Acad. Sci. U.S.A.*,  
517 117, 4505, <https://doi.org/10.1073/pnas.1919344117>, 2020.

518 Wang, S. and Wang, L.: The atmospheric oxidation of dimethyl, diethyl, and diisopropyl ethers. The role of the intramolecular  
519 hydrogen shift in peroxy radicals, *Phys. Chem. Chem. Phys.*, 18, 7707-7714, <https://doi.org/10.1039/C5CP07199B>, 2016.

520 Wang, S., Riva, M., Yan, C., Ehn, M., and Wang, L.: Primary Formation of Highly Oxidized Multifunctional Products in the  
521 OH-Initiated Oxidation of Isoprene: A Combined Theoretical and Experimental Study, *Environ. Sci. Technol.*, 52, 12255-  
522 12264, <https://doi.org/10.1021/acs.est.8b02783>, 2018.

523 Wang, S., Wu, R., Berndt, T., Ehn, M., and Wang, L.: Formation of Highly Oxidized Radicals and Multifunctional Products  
524 from the Atmospheric Oxidation of Alkylbenzenes, *Environ. Sci. Technol.*, 51, 8442-8449,  
525 <https://doi.org/10.1021/acs.est.7b02374>, 2017.

526 Wang, K., Wang, W. G., Fan, C. C.: Reactions of C<sub>12</sub>-C<sub>14</sub> N-Alkylcyclohexanes with Cl Atoms: Kinetics and Secondary  
527 Organic Aerosol Formation, *Environ. Sci. Technol.*, 56(8): 4859-4870, <https://doi.org/10.1021/acs.est.1c08958>, 2022.

528 Wu, R., Wang, S., and Wang, L.: New Mechanism for the Atmospheric Oxidation of Dimethyl Sulfide. The Importance of  
529 Intramolecular Hydrogen Shift in a CH<sub>3</sub>SCH<sub>2</sub>OO Radical, *J. Phys. Chem. A*, 119, 112-117, <https://doi.org/10.1021/jp511616j>,  
530 2015.

531 Xia, M., Peng, X., Wang, W.: Significant Production of ClNO<sub>2</sub> and Possible Source of Cl<sub>2</sub> from N<sub>2</sub>O<sub>5</sub> Uptake at a Suburban  
532 Site in Eastern China, *Atmos. Chem. Phys.*, 20(10): 6147-6158, <https://doi.org/10.1021/10.5194/acp-20-6147-2020>, 2020.

533 Xie, H. B., Ma, F.F., Yu, Q., He, N., and Chen, J. W.: Computational Study of the Reactions of Chlorine Radicals with  
534 Atmospheric Organic Compounds Featuring  $\text{NH}_x$ - $\pi$ -Bond ( $x = 1, 2$ ) Structures, *J. Phys. Chem. A*, 121, 1657-1665,  
535 <https://doi.org/10.1021/acs.jpca.6b11418>, 2017.

536 Xie, H. B., Li, C., He, N., Wang, C., Zhang, S., and Chen, J. W.: Atmospheric Chemical Reactions of Monoethanolamine  
537 Initiated by OH Radical: Mechanistic and Kinetic Study, *Environ. Sci. Technol.*, 48, 1700-1706,  
538 <https://doi.org/10.1021/es405110t>, 2014.

539 Xie, H. B., Ma, F.F., Wang, Y., He, N., Yu, Q., and Chen, J. W.: Quantum Chemical Study on  $\cdot\text{Cl}$ -Initiated Atmospheric  
540 Degradation of Monoethanolamine, *Environ. Sci. Technol.*, 49, 13246-13255, <https://doi.org/10.1021/acs.est.5b03324>, 2015.

541 Young, C. J., Washenfelder, R. A., Edwards, P. M., Parrish, D. D., Gilman, J. B., Kuster, W. C., Mielke, L. H., Osthoff, H. D.,  
542 Tsai, C., Pikelnaya, O., Stutz, J., Veres, P. R., Roberts, J. M., Griffith, S., Dusanter, S., Stevens, P. S., Flynn, J., Grossberg,  
543 N., Lefer, B., Holloway, J. S., Peischl, J., Ryerson, T. B., Atlas, E. L., Blake, D. R., and Brown, S. S.: Chlorine as a primary  
544 radical: evaluation of methods to understand its role in initiation of oxidative cycles, *Atmos. Chem. Phys.*, 14, 3427-3440,  
545 <https://doi.org/10.5194/acp-14-3427-2014>, 2014.

546 Yu, D., Tan, Z., Lu, K., Ma, X., Li, X., Chen, S., Zhu, B., Lin, L., Li, Y., Qiu, P., Yang, X., Liu, Y., Wang, H., He, L., Huang,  
547 X., and Zhang, Y.: An explicit study of local ozone budget and  $\text{NO}_x$ -VOCs sensitivity in Shenzhen China, *Atmos. Environ.*,  
548 224, 117304, <https://doi.org/10.1016/j.atmosenv.2020.117304>, 2020.

549 Yu, F. and Luo, G.: Modeling of gaseous methylamines in the global atmosphere: impacts of oxidation and aerosol uptake,  
550 *Atmos. Chem. Phys.*, 14, 12455-12464, <https://doi.org/10.5194/acp-14-12455-2014>, 2014.

551 Yu, Q., Xie, H. B., and Chen, J. W.: Atmospheric chemical reactions of alternatives of polybrominated diphenyl ethers initiated  
552 by OH: A case study on triphenyl phosphate, *Sci. Total Environ.*, 571, 1105-1114,  
553 <https://doi.org/10.1016/j.scitotenv.2016.07.105>, 2016.

554 Yu, Q., Xie, H. B., Li, T., Ma, F., Fu, Z., Wang, Z., Li, C., Fu, Z., Xia, D., and Chen, J. W.: Atmospheric chemical reaction  
555 mechanism and kinetics of 1,2-bis(2,4,6-tribromophenoxy)ethane initiated by OH radical: a computational study, *RSC Adv.*,  
556 7, 9484-9494, <https://doi.org/10.1039/C6RA26700A>, 2017.

557 Yuan, B., Coggon, M. M., Koss, A. R., Warneke, C., Eilerman, S., Peischl, J., Aikin, K. C., Ryerson, T. B., and de Gouw, J.  
558 A.: Emissions of volatile organic compounds (VOCs) from concentrated animal feeding operations (CAFOs): chemical  
559 compositions and separation of sources, *Atmos. Chem. Phys.*, 17, 4945-4956, <https://doi.org/10.5194/acp-17-4945-2017>, 2017.

560 Zhang, R., Wang, G., Guo, S., Zamora, M. L., Ying, Q., Lin, Y., Wang, W., Hu, M., and Wang, Y.: Formation of Urban Fine  
561 Particulate Matter, *Chem. Rev.*, 115, 3803-3855, <https://doi.org/10.1021/acs.chemrev.5b00067>, 2015.

562 Zhang, Z., Lin, L., and Wang, L.: Atmospheric oxidation mechanism of naphthalene initiated by OH radical. A theoretical  
563 study, *Phys. Chem. Chem. Phys.*, 14, 2645-2650, <https://doi.org/10.1039/C2CP23271E>, 2012.

564 Zhao, Y. and Truhlar, D. G.: The M06 suite of density functionals for main group thermochemistry, thermochemical kinetics,  
565 noncovalent interactions, excited states, and transition elements: two new functionals and systematic testing of four M06-class  
566 functionals and 12 other functionals, *Theor. Chem. Acc.*, 120, 215-241, <https://doi.org/10.1007/s00214-007-0310-x>, 2008.

567 Zito, P., Dötterl, S., and Sajevo, M.: Floral Volatiles in a Sapromyiophilous Plant and Their Importance in Attracting House  
568 Fly Pollinators, *J. Chem. Ecol.*, 41, 340-349, <https://doi.org/10.1007/s10886-015-0568-8>, 2015.